Applied Surface Science 462 (2018) 565–574

Contents lists available at ScienceDirect

Applied Surface Science

journal homepage: www.elsevier.com/locate/apsusc

Full Length Article

Multi-scale dimple creation on metallic glass by a two-step method involving nanoindentation and polishing

Hu Huang[a,b,*], Jiwang Yan[b,*]

[a] School of Mechanical Science and Engineering, Jilin University, Changchun, Jilin 130022, China
[b] Department of Mechanical Engineering, Faculty of Science and Technology, Keio University, Yokohama 223-8522, Japan

ARTICLE INFO

Keywords:
Metallic glass
Multi-scale dimple
Nanoindentation
Pre-indent
Polishing

ABSTRACT

Creation of micro dimples on material surface is significant for their functional applications. Because of unique properties, metallic glasses are regarded as emerging structural and functional materials but they are also a kind of difficult-to-cut materials due to high hardness and easy to crystallization and oxidation. In this study, a new method was proposed to fabricate micro dimples on metallic glass surface, which consisted of two steps, nanoindentation experiments to form the pre-indent array followed by polishing. Via this two-step method, square and rectangle dimples were successfully formed which exhibited multi-scale features with one relatively large dimple with width in micron-scale and depth in nanometer-scale, together with relatively small residual indents in nanometer-scale distributed on its bottom surface. The experimental results indicated that the depth of multi-scale dimples was affected by the spatial interval between two indents and the polishing time. Under the used experimental conditions, for the same polishing time, the depth of the large dimple was decreased when increasing the interval; for the same interval, with increase in the polishing time, the depth of the large dimple was also decreased. The possible formation mechanism of the large dimple was discussed, which was mainly ascribed to the enhanced material removal at the position of pre-indent array because of the concentration of polishing particles by the pre-indents.

1. Introduction

Being an amorphous atomic structure, metallic glasses (MGs) possess attractive mechanical, physical, and chemical properties, such as high hardness, strength, elastic limit, and good resistance to wear and corrosion [1–4]. Thus, they are regarded as emerging structural and functional materials. For example, they are promising materials for spacecrafts because of high strength that can greatly reduce the weight; the high hardness and wear resistance make MGs become excellent mold materials [5]; taking features of high strength and low elastic modulus, MGs also show huge potential for biomedical applications [6]; the good resistance to corrosion makes MGs good candidates for using in micro/nano-fluidic devices [7].

On the other hand, it is commonly reported that surface microstructures can provide some novel optical, physical, and biomedical functions and properties for materials [7–14]. Micro dimple is a typical surface structure, which is widely employed in micro-molds, micro-mechanical systems, micro/nano-fluidic devices, and bionic functional surfaces. Although thermoplastic forming in the supercooled liquid region (SLR) provides a unique way to shape MGs into various products [11,15,16], this method requires expensive molds, and crystallization may occur because the forming temperature is quite difficult to control especially for the MGs with a narrow SLR [2,17]. Moreover, due to the capillary effect and other reasons, MG materials are difficult to completely fill the micro/nano-structured molds [9,10,15]. Another problem exists in the demolding process where etching of the mold by acid or alkali is commonly used [10,15,16,18], further increasing the cost and also polluting the environment. In addition, although mechanical machining for example diamond cutting is a flexible method to fabricate microstructures on material surface [13,19,20], some issues such as severe tool wear because of high hardness of MGs, crystallization and oxidation due to high local temperature because of very low thermal conductivity of MGs [21–23], and generation of shear bands around the formed structure [24], limit its application in fabricating micro dimples on MG surface. The energy-based machining methods such as electrical discharge and laser machining can easily produce microstructures on MG surface [8,25], but crystallization is still a significant problem [8,25–27]. Moreover, burrs and pile-ups commonly appear around the microstructure fabricated by diamond cutting and energy-based machining methods [26,28,29], which reduce the performance of the

* Corresponding authors at: School of Mechanical Science and Engineering, Jilin University, Changchun, Jilin 130022, China (H. Huang).
E-mail addresses: huanghu@jlu.edu.cn (H. Huang), yan@mech.keio.ac.jp (J. Yan).

https://doi.org/10.1016/j.apsusc.2018.08.180
Received 15 May 2018; Received in revised form 24 July 2018; Accepted 21 August 2018
Available online 23 August 2018
0169-4332/

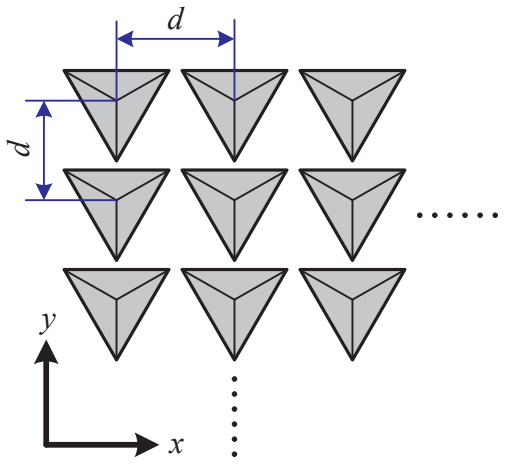

Fig. 1. Schematic diagram illustrating the formation of pre-indent array.

structured surface. Therefore, new methods to fabricate micro dimples on MG surface should be further explored.

Nanoindentation is a widely used method to characterize the mechanical properties of materials in micro/nano-scale [30]. After nanoindentation, residual indent with depth in micro/nano-scale is formed on the sample surface. Accordingly, nanoindentation has also been employed to form micro dimples on material surface by directly penetrating the indenter into the sample [31]. However, because of the material extrusion due to the strong interaction between the indenter and sample surfaces, pile-ups were also observed [32,33] especially for metal materials and thus further surface treatment is required. In the daily experiments, when re-polishing the indented sample surface for reuse, it is observed that micro dimple with depth in micro/nano-scale could be formed at the position of residual indent. If pre-indent array with controlled spatial interval between two indents is produced on MG surface prior to polishing, one relatively large dimple with width in micron-scale and depth in nanometer-scale, together with relatively small residual indents in nanometer-scale distributed on its bottom surface, i.e., a multi-scale dimple, could be created on the MG surface. According to this idea, fabrication of multi-scale dimples on Zr-based MG surface was attempted in this study by a two-step method involving nanoindentation and polishing. Experimental results showed that multi-scale square and rectangle dimples were successfully formed, verifying the validity of the proposed method.

2. Materials and experiments

A Zr-based MG, $Zr_{41.2}Ti_{13.8}Cu_{12.5}Ni_{10}Be_{22.5}$ (commonly called Vitreloy 1) was used in this study. One sample with a thickness of 1 mm and diameter of 10 mm was cut from an as-cast MG rod by wire electrical discharge machining (wire-EDM). To remove the crystallization layer formed during EDM [25,26] and at the same time improve the surface quality for subsequent nanoindentation experiments, the sample was mechanically ground using 400, 800, and 1500 grit sand papers in sequence and then polished using Al_2O_3 polishing suspension (3.0 CR, 1.0 CR, and 0.3 CR with nominal particle size of 3.0 μm,

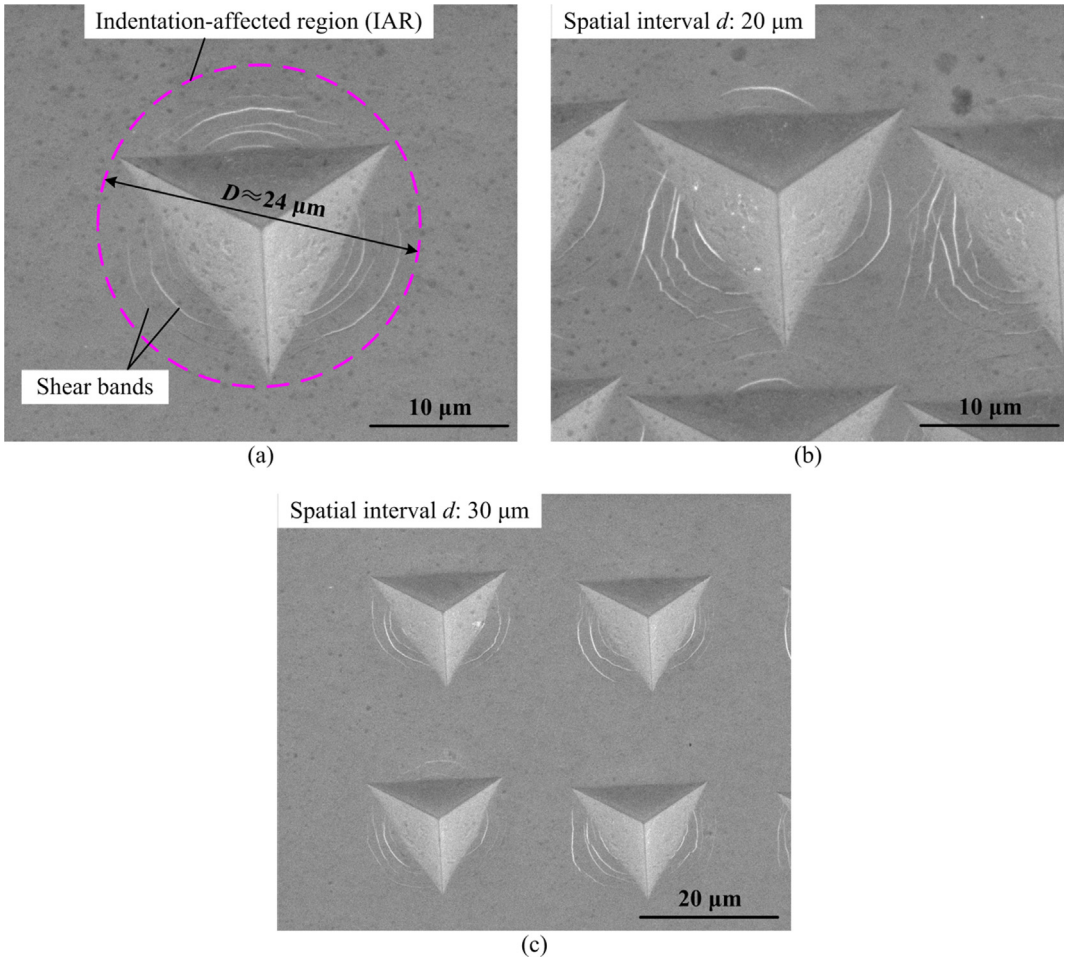

Fig. 2. (a) SEM morphology of a single indent formed under the maximum indentation load of 1000 mN and loading/unloading rate of 100 mN/s; (b) and (c) SEM morphologies of the pre-indent arrays with different spatial intervals *d*: (b) 20 μm and (c) 30 μm.

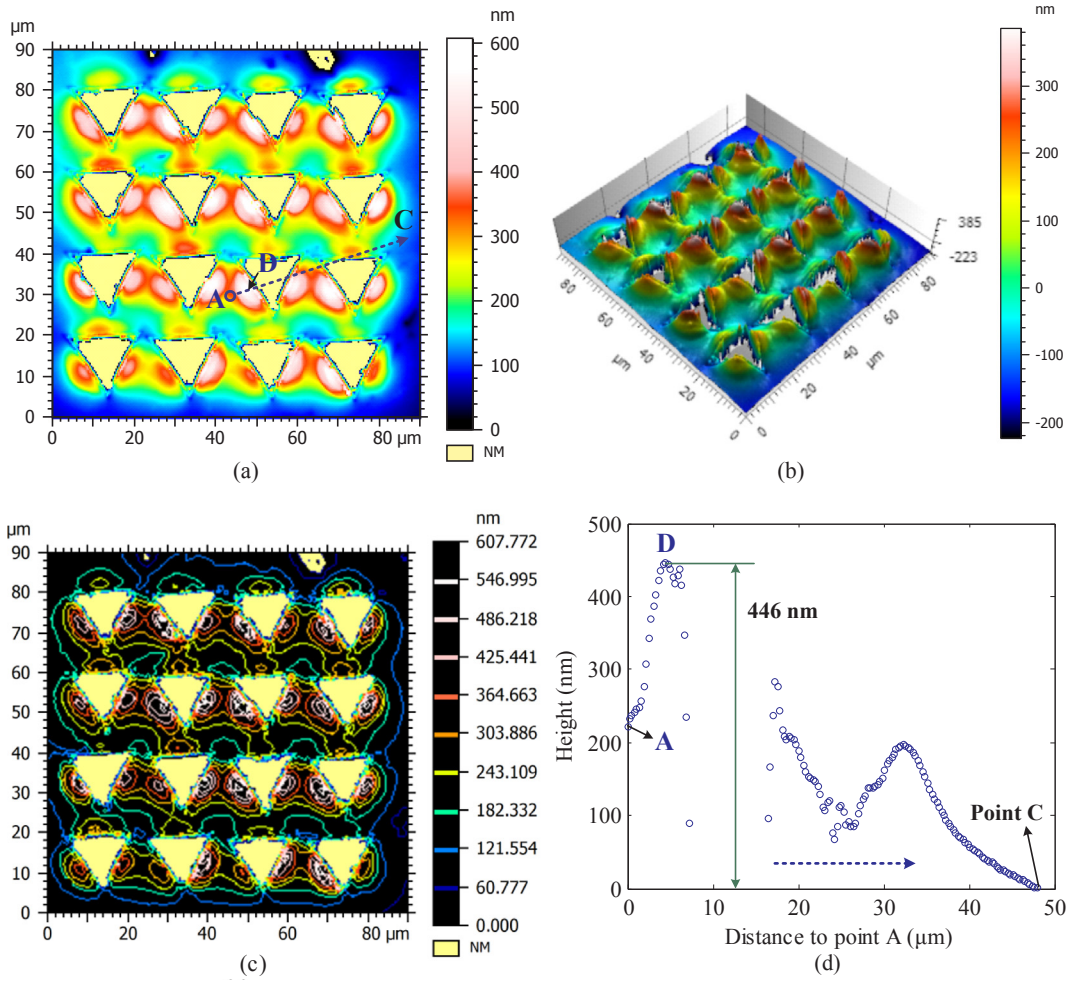

Fig. 3. (a) and (b) 3D topographies of the 4 × 4 pre-indent array formed under an interval *d* of 20 μm, (c) the corresponding contour, and (d) the profile of the dotted line in Fig. 3(a).

1.0 μm, and 0.3 μm respectively, Baikalox CR, Baikowski, France) mixed with water at the ratio of 1:2 in sequence. The polishing pressure was about 0.64 MPa evaluated by the force due to the weight of the holder divided by the polishing area.

Pre-indent arrays were produced on the polished MG surface by using a commercial nanoindentation instrument (ENT-1100, Elionix Inc., Japan) equipped with a Berkovich type diamond indenter. As illustrated in Fig. 1, by varying the spatial interval *d* between two indents and the number of indents along *x* or *y* axis, the dimension and shape of the pre-indent array can be tuned. The maximum indentation load of 1000 mN was used and the loading/unloading rate of 100 mN/s was selected to reduce the total nanoindentation time. To select the interval *d*, single nanoindentation experiment was performed under the above mentioned experimental conditions, and the corresponding length of indent edges and indentation-affected region (IAR) were determined to be about 20 and 24 μm, respectively. Accordingly, as examples, 4 × 4 square arrays with different intervals *d* (20, 50, and 80 μm) and 10 × 4 rectangle array with an interval *d* of 30 μm were formed on the MG surface.

After nanoindentation experiments, the pre-indent arrays were observed by using an environmental scanning electron microscope (ESEM) (Inspect S50, FEI, USA) and the corresponding three dimensional (3D) topographies were measured by using a white light interferometer (Talysurf CCI1000, AMETEK Taylor Hobson Ltd., UK). After characterizing the surface features of pre-indent arrays, the indented surface was further polished for about 15 min by using 0.3 μm Al_2O_3 polishing suspension. Then, the polished surface was cleaned by acetone using cotton swabs followed by ultrasonic cleaner for 5 min. The 3D topographies of the indented regions after polishing were measured by the white light interferometer again. To study the effect of polishing time on the results, a 4 × 4 square array with the interval *d* of 50 μm was polished for about 10 min and then characterized for comparison.

3. Results and discussion

Fig. 2(a) shows the SEM morphology of a single indent formed under the maximum indentation load of 1000 mN and loading/unloading rate of 100 mN/s. An inverted pyramid indent is observed, which is surrounded by some semicircle shear bands generated due to the amorphous structure of MG. Using a circle to surround the indent and shear bands, the size of the IAR is roughly evaluated to be 24 μm. According to the scale bar, the length of indent edges is calculated to be about 20 μm. Fig. 2(b) presents a typical SEM morphology of pre-indent array when the interval *d* is 20 μm, being less than the diameter of the IAR. As portion of the subsequent indent is still in the IAR of the preceding one, the shape of shear bands has been significantly affected due to the interaction between two IARs [34] and some straight shear bands appear. When the interval *d* is increased to 30 μm, the interaction between two IARs is weakened and shear bands almost recover to semicircle as shown in Fig. 2(c). With further increasing of the interval to 50 and 80 μm, the shear bands of the pre-indent arrays (not given here) exhibit the same features to that of the single indent in Fig. 2(a).

Fig. 3(a) and (b) present typical 3D topographies of the 4 × 4 pre-

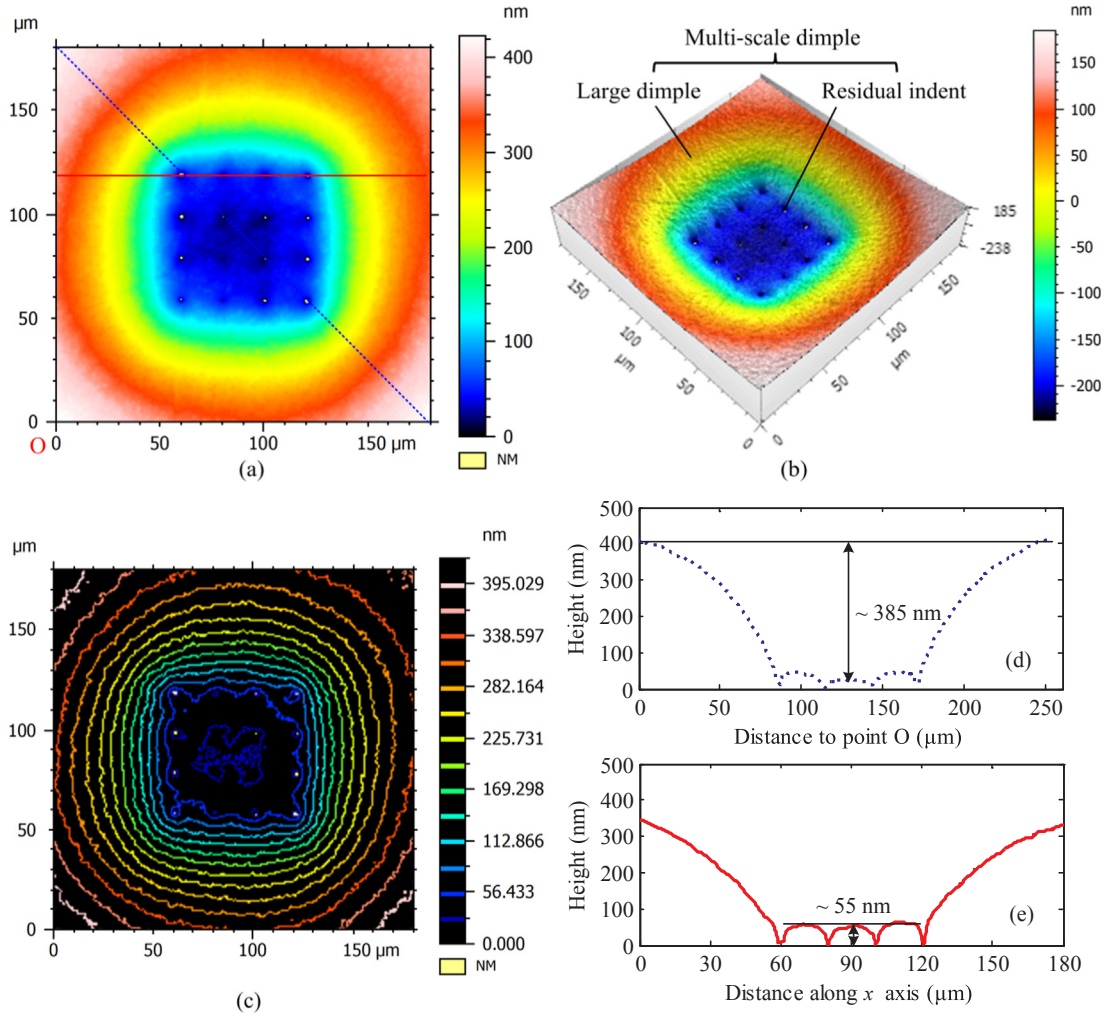

Fig. 4. (a) and (b) 3D topographies of the 4 × 4 pre-indent array (d = 20 μm) after polishing for 15 min, (c) the corresponding contour, (d) and (e) profiles of the dotted line and solid line in Fig. 4(a), respectively.

indent array formed under an interval of 20 μm. Fig. 3(c) shows the corresponding contour and Fig. 3(d) illustrates the profile of the dotted line in Fig. 3(a). It is noted that the height around the edges of pre-indents is considerable higher than that of the initial surface. For example, in Fig. 3(d), the height of point D (around the edge of the pre-indent) is about 446 nm higher than that of point C (initial surface). This phenomenon is the so-called "pile-up" in the field of nanoindentation [32,33], which results from the strong interaction between the indenter and material surface that induces the plastic extrusion of materials. From Figs. 2 and 3, it is noted that although single/array micro dimple can be generated on the MG surface by nanoindentation, a large number of surface defects such as shear bands and pile-ups appear around the dimple. Thus, it is not feasible to obtain micro dimple free of surface defects around by only using nanoindentation.

Figs. 4, 5, and 6 show the surface features of pre-indent arrays after polishing for 15 min, and the corresponding intervals d are 20, 50, and 80 μm, respectively. It is noted that the pile-up as shown in Fig. 3 has been removed and the triangle-shape of pre-indents disappears. When the intervals are 20 and 50 μm, relatively large dimples with width of hundreds of micrometers are clearly observed at the positions of pre-indent arrays as shown in Figs. 4(a)–(c), 5(a), and (b). The corresponding depth of the large dimple near the center is about 385 nm when d is 20 μm, and it is decreased to about 240 nm when d is increased to 50 μm. Apart from the large dimple, dimple-like residual indents are distributed on the bottom surface of the large dimple. Correspondingly, the measured depth of residual indent is about 55 nm when d is 20 μm, being less than that when d is 50 μm (about 140 nm). Although there may be some errors when measuring the depth of residual indent because (1) some small particles remain at the tip of residual indent being difficult to clean and (2) the tip of residual indent is very sharp that affects the optical measurement, the change in depth of residual indent suggests the same tendency that the decrease in the interval d increases the depth of the large dimple.

Furthermore, when d is increased to 80 μm, as shown in Fig. 6, the large dimple is extremely shallow and it is very hard to identify its shape from the 3D topographies in Fig. 6(a) and (b). On the contrary, the dimple shape of the relatively small residual indents becomes clear after polishing. From Fig. 6(d), it is obtained that the depth of the large dimple is only about 40 nm and it is around 180 nm for residual indent.

The results shown in Figs. 4–6 are obtained by polishing the 4 × 4 square pre-indent arrays and the only difference in experimental condition is the interval d. These results confirm that multi-scale square dimples with one relatively large dimple in micron-scale width and nanometer-scale depth as well as relatively small residual indents in nanometer-scale depth can be fabricated on MG surface by the proposed two-step method, i.e., nanoindentation experiments to form the pre-indent array followed by polishing. The depth of the multi-scale square dimple strongly depends on the interval d of pre-indents. To further verify the validity of the two-step method, Fig. 7 shows the surface features of a 10 × 4 rectangle pre-indent array (d = 30 μm) after polishing for 15 min. The results confirm that a multi-scale rectangle

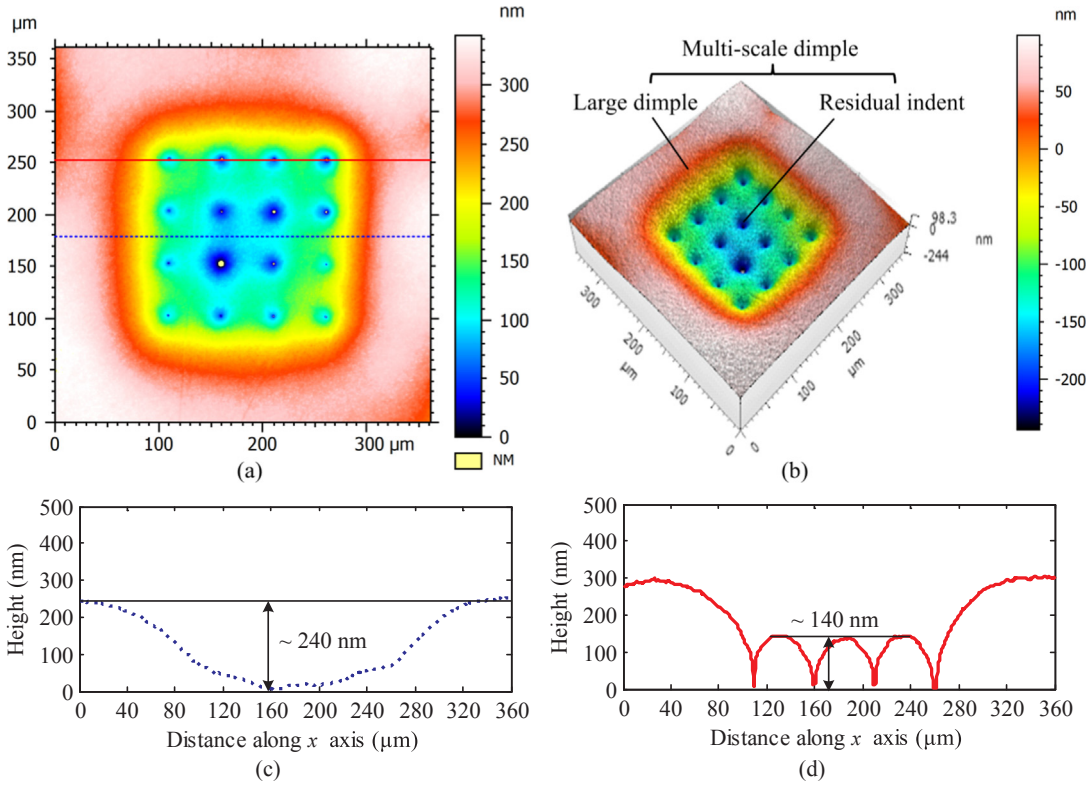

Fig. 5. (a) and (b) 3D topographies of the 4 × 4 pre-indent array (d = 50 μm) after polishing for 15 min, (c) and (d) profiles of the dotted line and solid line in Fig. 5(a), respectively.

dimple has been successfully fabricated on the MG surface. The corresponding depth of the large dimple is about 340 nm and the depth of residual indent is about 80 nm. Furthermore, as the interval d (30 μm) is between 20 and 50 μm, the depth of the large dimple is a little larger than that of the multi-scale square dimple in Fig. 5 (d = 50 μm) but a little smaller than that of the one in Fig. 4 (d = 20 μm). The comparison of the depth of residual indent also shows the same tendency.

As the validity of the two-step method has been confirmed by the aforementioned results, next we will study the effect of polishing time on the multi-scale dimple. Fig. 8 shows the surface features of a 4 × 4 square pre-indent array (d = 50 μm) after polishing for 10 min. For comparison, all the other experimental conditions in Fig. 8 are the same with those in Fig. 5 except for the polishing time. It is interesting to find that after polishing for 10 min, both the depth of the large dimple (about 300 nm) and the depth of residual indent (about 160 nm) are larger than those after polishing for 15 min (about 240 and 140 nm, respectively). This suggests that during the increased polishing time of 5 min, the MG materials on both the surrounded surface and the surface between pre-indents are removed simultaneously, and the material removal rate of the surrounded surface is larger than that of the surface between pre-indents.

In summary, Table 1 lists the main results obtained from Figs. 4–8. It can be concluded that for the same polishing time of 15 min, increasing the interval d from 20 to 80 μm results in decreasing of the depth of the large dimple from 385 to 40 nm but increasing of the depth of residual indent from 55 to 180 nm; for the same interval d of 50 μm, when increasing the polishing time from 10 to 15 min, the depth of the large dimple is decreased from 300 to 240 nm together with the decreasing of the depth of residual indent from 160 to 140 nm.

The formation of multi-scale dimple at the position of pre-indent array indicates that the pre-indent array has the function to enhance the material removal during subsequent polishing process. As the formation of residual indent is easily understood by non-complete removal of the pre-indent during polishing, the emphasis will focus on the formation mechanism of the large dimple by the two-step method, which will be helpful for explaining these results in Table 1. As the pre-indent array has been formed on the MG surface prior to polishing, the enhanced material removal at the position of pre-indent array during polishing may result from the following potential reasons: (1) the corrosion of polishing suspension [35–37], (2) the concentration of polishing particles due to the pre-indents, and (3) the residual stress induced via shear band creation during indentation [38–42].

Although MGs commonly exhibit good corrosion resistance, previous studies [35–37] indicated that the pitting corrosion could occur on shear bands of the pre-deformed MGs under certain conditions. As shear bands appear around the pre-indents and polishing suspension is used in our study, the role of polishing suspension on the material removal especially at the position of shear bands should be explored and clarified. For this purpose, the MG sample with pre-indents on its surface was immersed in the solution mixed by 15 ml Al_2O_3 polishing suspension and 15 ml water. To highlight the effect of polishing suspension, a higher volume percentage of polishing suspension (1:1) was used here. The immersed time was selected to the same with the polishing time of 15 min. Then, the sample surface was cleaned and observed again, and typical SEM morphologies of the indents before and after corrosion are shown in Fig. 9. It is observed that for both a single indent and the indent array (d = 20 μm), there is no visible difference in the morphologies obtained before and after corrosion except for some contaminants on the corroded surface. This result excludes the corrosion role of polishing suspension. Moreover, it has been experimentally confirmed that the multi-scale dimple can also be formed when using diamond abrasive paste, which further excludes the role of polishing suspension.

Another possible reason resulting in the enhanced material removal at the position of pre-indent array in polishing is the concentration of polishing particles due to the pre-indents, as illustrated in Fig. 10. In the initial state as illustrated in Fig. 10(a), because of the existing of pre-indent array, more polishing particles could be concentrated in the

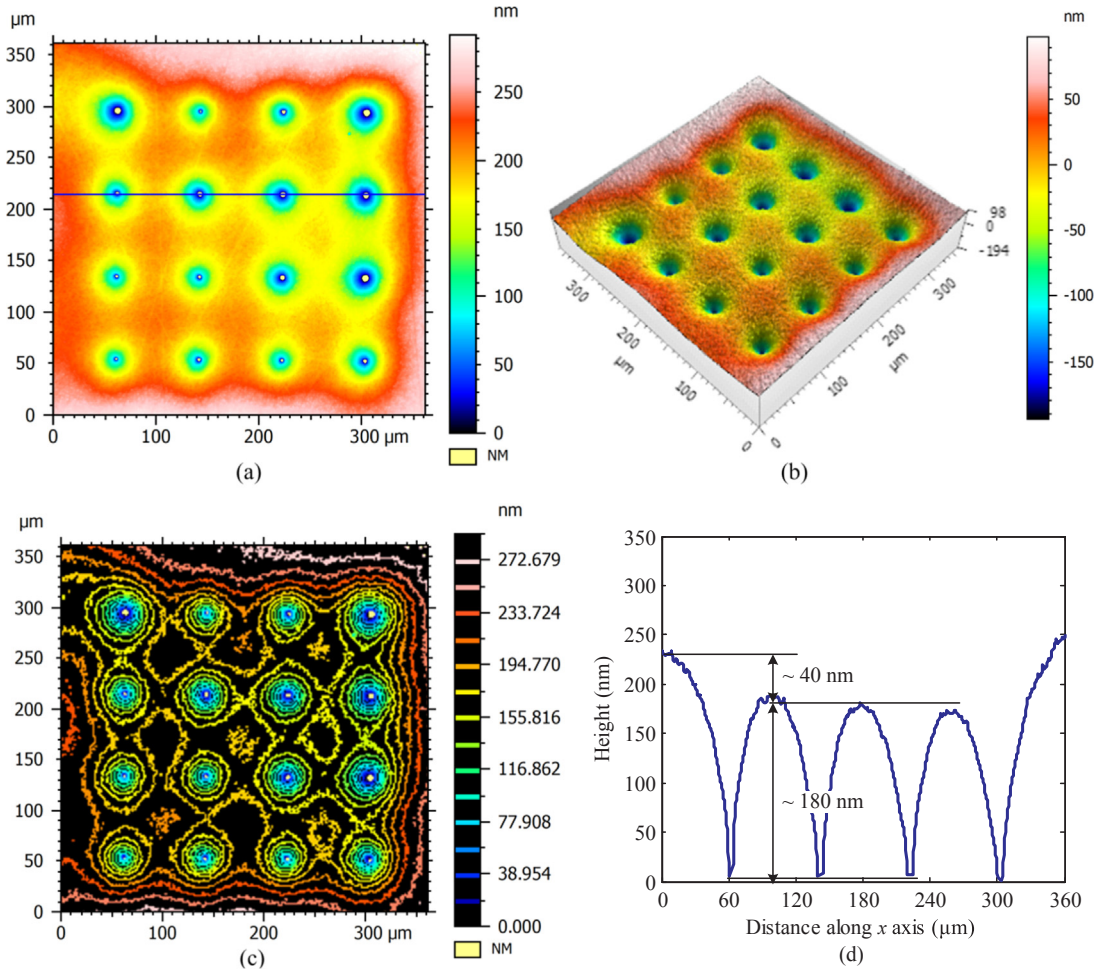

Fig. 6. (a) and (b) 3D topographies of the 4 × 4 pre-indent array (d = 80 μm) after polishing for 15 min, (c) the corresponding contour, and (d) profile of the solid line in Fig. 6(a).

indented region, which increases the effective interaction time and length between the polishing particles and the indented region. Thus, the material removal rate at the position of pre-indent array is slightly higher than that of the surrounded surface.

Because the pile-ups together with shear bands are higher than the surrounded polished surface, they are removed firstly. As time goes on, the pile-ups and shear bands are completely removed, and correspondingly, dimple-like residual indents as well as a very shallow large dimple are formed as illustrated in Fig. 10(b). Furthermore, rounded corners appear around the residual indent as shown in Figs. 4–8 due to the high material removal rate at the edge mainly because of the relatively high pressure at the edge of pre-indents during polishing [43]. With time, the depth of the large dimple is gradually increased because of the slightly higher material removal rate of the surface between pre-indents than that of the surrounded surface. At a certain time, the depth of the large dimple reaches a critical value as illustrated in Fig. 10(c). After that, the concentration role of polishing particles is significantly weakened because the residual depth of pre-indents is relatively small. Although the formed large dimple also has the role to concentrate the polishing particles, the pressure applied on the polishing particle by the large dimple and polishing pad has been significantly reduced because the relatively large gap between the large dimple and the polishing pad. These two aspects result in the material removal rate of the surface between pre-indents being smaller than that of the surrounded surface of the pre-indent array. This can explain the phenomenon that although the polishing time is increased from 10 to 15 min, the corresponding depth of the large dimple is decreased from 300 to 240 nm as shown in the comparative results in Figs. 5 and 8.

Furthermore, the change in depth of the large dimple with the interval d could also be rationalized as follows. From Fig. 10, it is easy to see that decreasing the interval d will increase the fraction of pre-indents per unit area; thus, the concentration of polishing particles can be effectively enhanced and relatively larger depth of the large dimple is achieved when d is 20 μm. On the contrary, if the interval d is too large, for example, 80 μm, the surface between pre-indents is almost the same with the surrounded surface of pre-indent array; thus, the concentration role of polishing particles is only limited around the individual pre-indent. This is why the depth of the large dimple is very shallow and dimple-like array appears when d is 80 μm, as shown in Fig. 6.

Additionally, the residual stress induced via shear band creation during indentation may also contribute to the formation of the large dimple, especially at the initial stage of polishing. Some previous studies [33,38,39] indicated that long-range internal stress fields may exist around the shear band, resulting in position-dependent fluctuations of nanoindentation hardness. By nanomechanical mapping around a single shear band formed by compression, hardness reduction at a micrometer length scale was reported [39], indicating the softening role of shear bands. As shear bands appear around the pre-indents as shown in Fig. 2, these regions with shear bands are relatively softer compared with the surrounded MG matrix. Therefore, during polishing, these regions distributed with shear bands are more easily removed, contributing to the formation of the large dimple at the initial stage. As the geometry of Berkovich type indenter is anisotropic, the residual stress around the pre-indent should be quite different, which can be

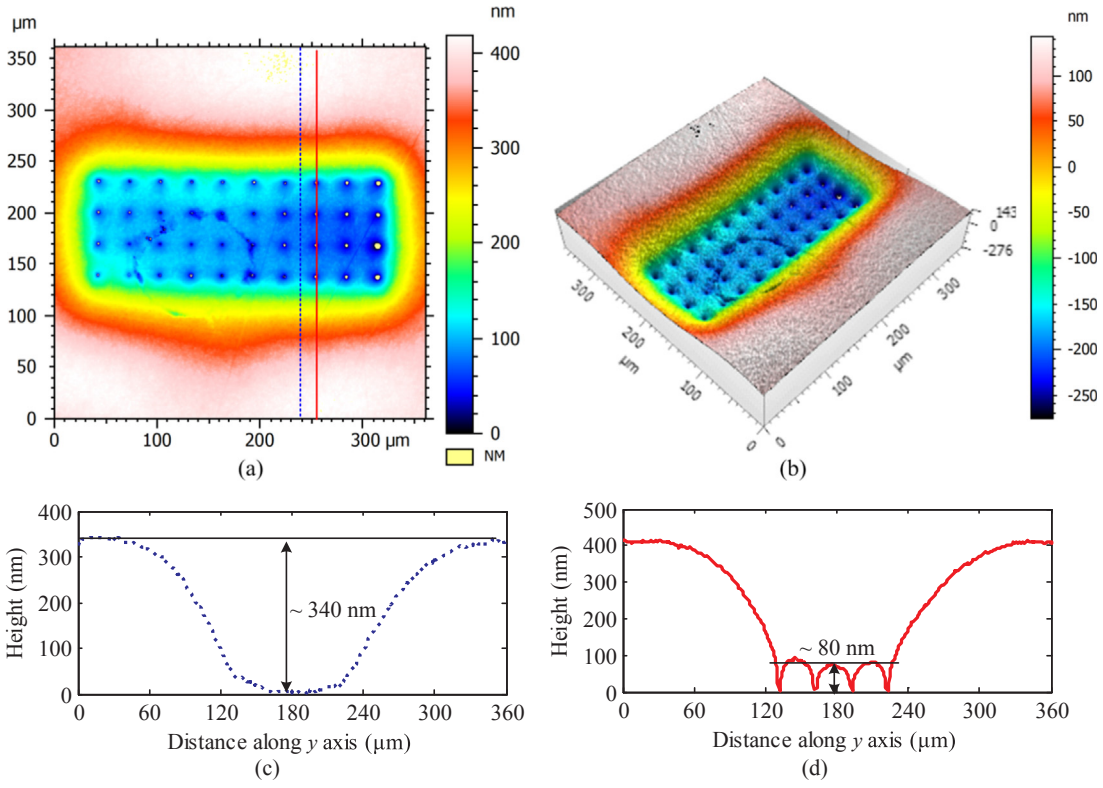

Fig. 7. (a) and (b) 3D topographies of the 10 × 4 pre-indent array (d = 30 μm) after polishing for 15 min, (c) and (d) profiles of the dotted line and solid line in Fig. 7(a), respectively.

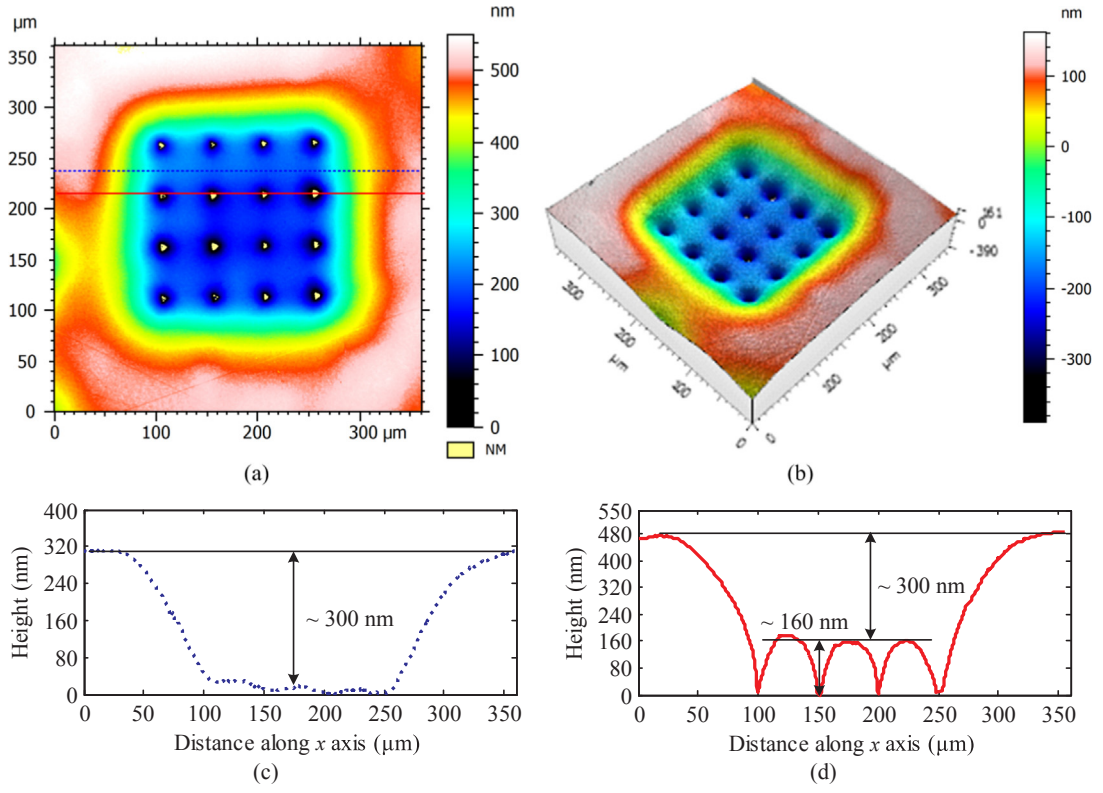

Fig. 8. (a) and (b) 3D topographies of the 4 × 4 pre-indent array (d = 50 μm) after polishing for 10 min, (c) and (d) profiles of the dotted line and solid line in Fig. 8(a), respectively.

Table 1
Summary of the results shown in Figs. 4–8.

Type of pre-indent array	Interval d, μm	Polishing time, minute	Depth of large dimple, nm	Depth of residual indent, nm
Square	20	15	385	55
Rectangle	30	15	340	80
Square	50	15	240	140
Square	80	15	40	180
Square	50	10	300	160

confirmed by the anisotropic distribution of pile-ups and shear bands around the pre-indent as shown in Figs. 2 and 3. However, in Fig. 6, it is noted that after polishing, the inverted pyramid shape of pre-indents has evolved to be the dimple shape, and the height distribution around the individual dimple is quite isotropic. This fact indicates that the difference in distribution of residual stress around the pre-indents has very slightly effect on the material removal during polishing, which indirectly implies that the role of the residual stress is relatively weak. If the role of residual stress is significant, the height distribution around the individual dimple in Fig. 6 should be non-uniform. Especially, when those regions with shear bands have been removed, the concentration role of polishing particles by the pre-indents as illustrated in Fig. 10 will become dominant.

Accordingly, the formation mechanism of the large dimple mentioned above could explain these results in Table 1 well. By varying the spatial interval between two indents and the number of indents along x and y axis, the geometric shape of the multi-scale dimple could be tuned. By varying the spatial interval and the polishing time, multi-scale dimples with various depth of large dimple and residual indent could be achieved.

Compared to the micro dimples formed by other methods, the multi-scale dimple created on MG surface by this two-step method shows smooth profiles free of pile-ups, burrs and shear bands around. Due to the very limited tensile plasticity of most MGs, their applications as practical structural materials have been greatly impeded. However, taking advantages of high hardness and wear resistance, MGs are good candidate materials for surface contact applications such as hydrostatic guide, bearing, cylinder and piston. For this kind of application, the multi-scale dimple structure with features of smooth profiles and non-burrs is beneficial to store gas or oil between contact surfaces without scratching the contact surface, which would promote fluid lubrication between contact surfaces and reduce the friction [29,44].

4. Conclusions

In summary, a two-step method, i.e., nanoindentation experiments to form the pre-indent array followed by polishing, was proposed and successfully used to fabricate square and rectangle dimples on MG surface. The created dimples showed multi-scale features with one relatively large dimple with width in micron-scale and depth in nanometer-scale, together with relatively small residual indents in nanometer-scale distributed on its bottom surface. Furthermore, the effects

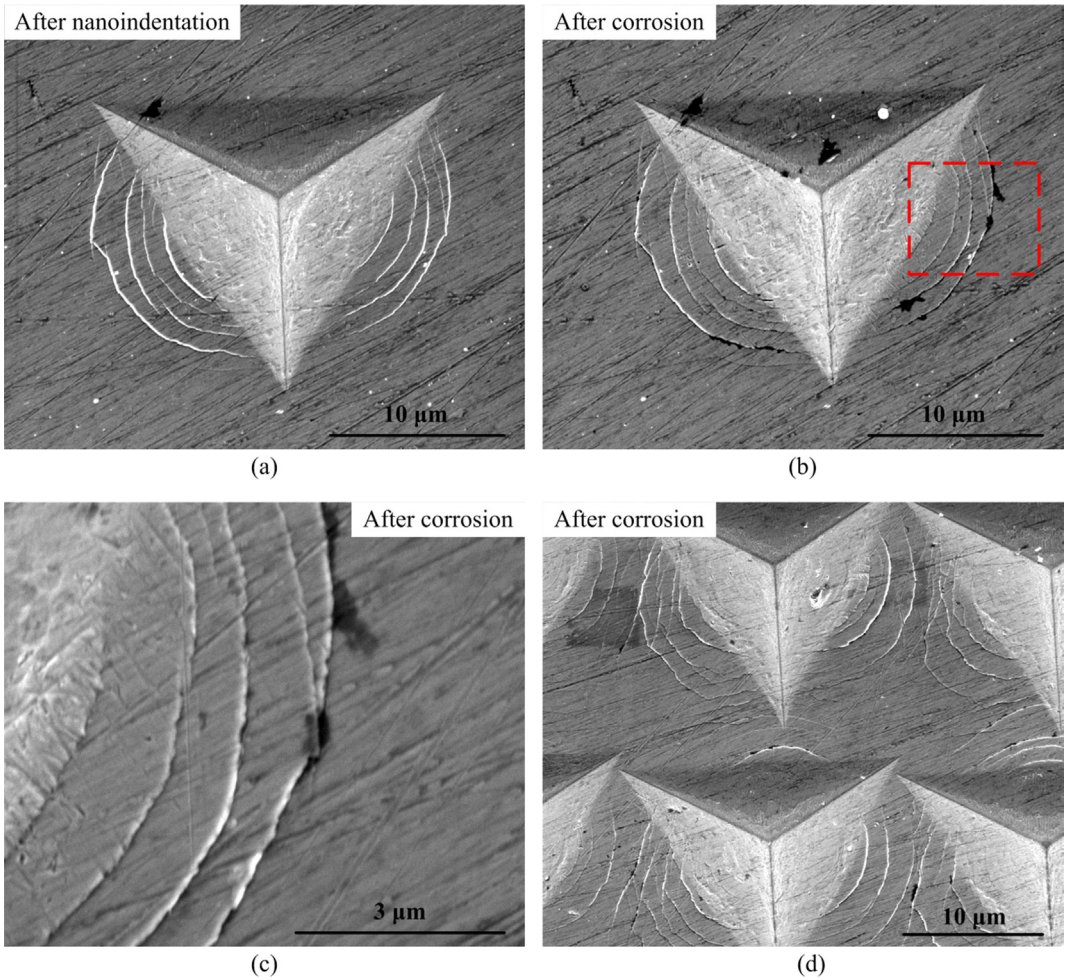

Fig. 9. SEM morphologies of an indent (a) after nanoindentation and (b) after corrosion, (c) local enlarged view of Fig. 9(b), and (d) SEM morphology of a pre-indent array (d = 20 μm) after corrosion.

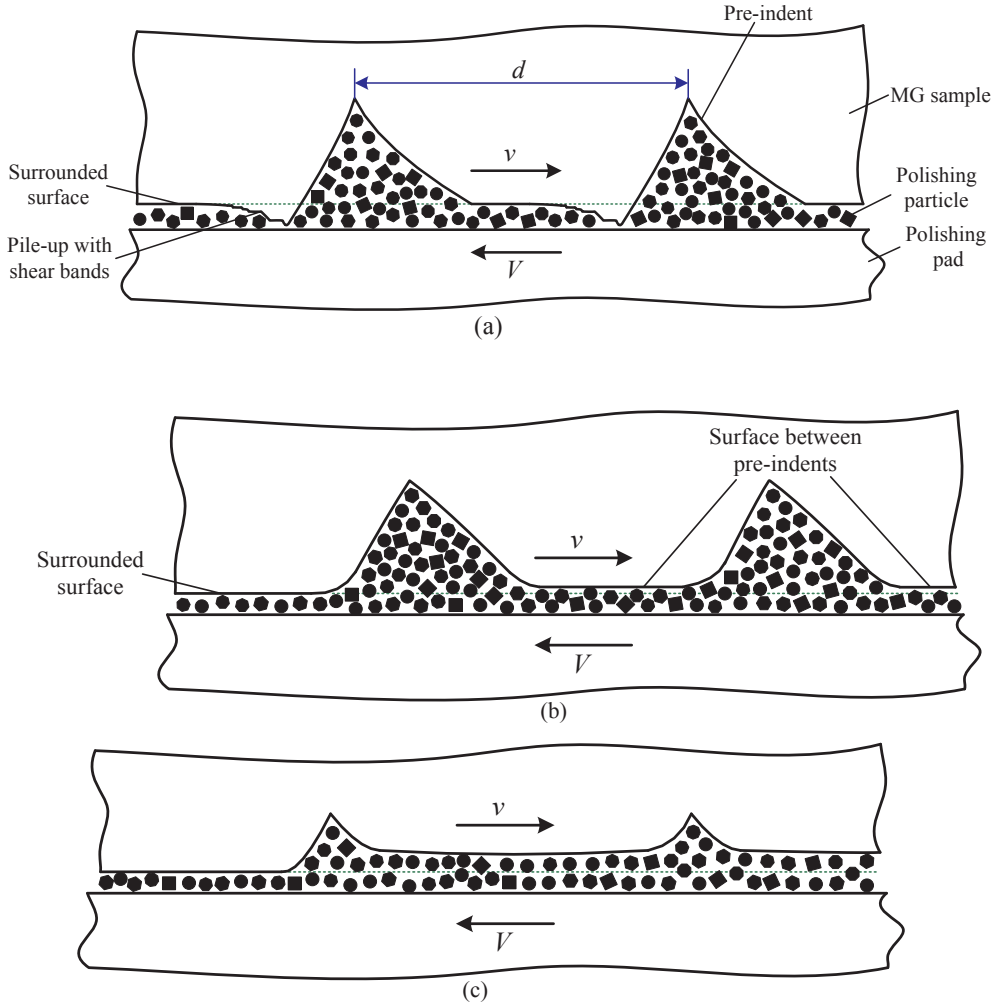

Fig. 10. Schematic diagram illustrating the enhanced material removal at the position of pre-indent array in polishing due to the concentration of polishing particles by the pre-indents: (a) the initial state, (b) the state after removing the pile-ups and shear bands, and (c) the state that the depth of the large dimple reaches a critical value.

of spatial interval between two indents and the polishing time on the depth of multi-scale dimples were studied. The results indicated that for the same polishing time of 15 min, increasing the interval from 20 to 80 μm resulted in decreasing of the depth of the large dimple from 385 to 40 nm but increasing of the depth of residual indent from 55 to 180 nm; for the same interval of 50 μm, when increasing the polishing time from 10 to 15 min, the depth of the large dimple was decreased from 300 to 240 nm together with the decreasing of the depth of residual indent from 160 to 140 nm. By analysis, the formation of the large dimple was mainly due to the concentration of polishing particles by the pre-indents, which enhanced the material removal at the position of pre-indent array during polishing. Apart from this reason, the residual stress induced via shear band creation during indentation may also contribute to the formation of the large dimple especially at the initial stage of polishing.

Acknowledgments

This work was supported by the National Natural Science Foundation of China (Grant No. 51705197), Young Elite Scientists Sponsorship Program by CAST (YESS) (Grant No. 2017QNRC001), Grant-in-Aid for JSPS Fellows (Grant No. 26-04048), and Fundamental Research Funds for the Central Universities.

References

[1] M.M. Trexler, N.N. Thadhani, Mechanical properties of bulk metallic glasses, Prog. Mater. Sci. 55 (2010) 759–839.
[2] J. Plummer, W.L. Johnson, Is metallic glass poised to come of age? Nat. Mater. 14 (2015) 553–555.
[3] C.J. Byrne, M. Eldrup, Materials science - bulk metallic glasses, Science 321 (2008) 502–503.
[4] W.H. Wang, The elastic properties, elastic models and elastic perspectives of metallic glasses, Prog. Mater. Sci. 57 (2012) 487–656.
[5] P. He, L.K. Li, F. Wang, O. Dambon, F. Klocke, K.M. Flores, A.Y. Yi, Bulk metallic glass mold for high volume fabrication of micro optics, Microsyst. Technol. 22 (2016) 617–623.
[6] H.F. Li, Y.F. Zheng, Recent advances in bulk metallic glasses for biomedical applications, Acta Biomater. 36 (2016) 1–20.
[7] F.Y. Wang, H. Zhang, X. Liang, F. Gong, J. Ma, Fabrication of metallic glass micro grooves by thermoplastic forming, J. Micromech. Microeng. 27 (2017) 025009.
[8] H. Huang, J.W. Yan, Surface patterning of Zr-based metallic glass by laser irradiation induced selective thermoplastic extrusion in nitrogen gas, J. Micromech. Microeng. 27 (2017) 075007.
[9] B. Sarac, S. Bera, S. Balakin, M. Stoica, M. Calin, J. Eckert, Hierarchical surface patterning of Ni- and Be-free Ti- and Zr-based bulk metallic glasses by thermoplastic net-shaping, Mat. Sci. Eng. C-Mater. 73 (2017) 398–405.
[10] Z. Liu, J. Schroers, General nanomoulding with bulk metallic glasses, Nanotechnology 26 (2015) 145301.
[11] J. Ma, X.Y. Zhang, D.P. Wang, D.Q. Zhao, D.W. Ding, K. Liu, W.H. Wang, Superhydrophobic metallic glass surface with superior mechanical stability and corrosion resistance, Appl. Phys. Lett. 104 (2014) 173701.
[12] N. Chen, X.T. Shi, R. Witte, K.S. Nakayama, K. Ohmura, H.K. Wu, A. Takeuchi, H. Hahn, M. Esashi, H. Gleiter, A. Inoue, D.V. Louzguine, A novel Ti-based nanoglass composite with submicron-nanometer-sized hierarchical structures to modulate osteoblast behaviors, J. Mater. Chem. B 1 (2013) 2568–2574.

[13] Z.W. Zhu, S. To, S.J. Zhang, Active control of residual tool marks for freeform optics functionalization by novel biaxial servo assisted fly cutting, Appl. Opt. 54 (2015) 7656–7662.
[14] Z.W. Han, Z.Z. Mu, W. Yin, W. Li, S.C. Niu, J.Q. Zhang, L.Q. Ren, Biomimetic multifunctional surfaces inspired from animals, Adv. Colloid Interface Sci. 234 (2016) 27–50.
[15] G. Kumar, H.X. Tang, J. Schroers, Nanomoulding with amorphous metals, Nature 457 (2009) 868–872.
[16] T. Xia, N. Li, Y. Wu, L. Liu, Patterned superhydrophobic surface based on Pd-based metallic glass, Appl. Phys. Lett. 101 (2012) 081601.
[17] G. Kaltenboeck, T. Harris, K. Sun, T. Tran, G. Chang, J.P. Schramm, M.D. Demetriou, W.L. Johnson, Accessing thermoplastic processing windows in metallic glasses using rapid capacitive discharge, Sci. Rep. 4 (2014) 6441.
[18] M. Hasan, G. Kumar, High strain rate thermoplastic demolding of metallic glasses, Scr. Mater. 123 (2016) 140–143.
[19] M. Mukaida, J.W. Yan, Ductile machining of single-crystal silicon for microlens arrays by ultraprecision diamond turning using a slow tool servo, Int. J. Mach. Tool. Manuf. 115 (2017) 2–14.
[20] Z.W. Zhu, S. To, K.F. Ehmann, G.B. Xiao, W.L. Zhu, A novel diamond micro-/nano-machining process for the generation of hierarchical micro-/nano-structures, J. Micromech. Microeng. 26 (2016) 035009.
[21] M. Bakkal, A.J. Shih, R.O. Scattergood, Chip formation, cutting forces, and tool wear in turning of Zr-based bulk metallic glass, Int. J. Mach. Tool. Manuf. 44 (2004) 915–925.
[22] K. Fujita, Y. Morishita, N. Nishiyama, H. Kimura, A. Inoue, Cutting characteristics of bulk metallic glass, Mater. Trans. 46 (2005) 2856–2863.
[23] M. Bakkal, C.T. Liu, T.R. Watkins, R.O. Scattergood, A.J. Shih, Oxidation and crystallization of Zr-based bulk metallic glass due to machining, Intermetallics 12 (2004) 195–204.
[24] H. Huang, H.W. Zhao, B.D. Wu, S.G. Wan, C.L. Shi, A novel two-axis load sensor designed for in situ scratch testing inside scanning electron microscopes, Sensors 13 (2013) 2552–2565.
[25] H. Huang, J.W. Yan, Microstructural changes of Zr-based metallic glass during microelectrical discharge machining and grinding by a sintered diamond tool, J. Alloys Compd. 688 (2016) 14–21.
[26] H. Huang, J.W. Yan, On the surface characteristics of a Zr-based bulk metallic glass processed by microelectrical discharge machining, Appl. Surf. Sci. 355 (2015) 1306–1315.
[27] H. Huang, J. Noguchi, J.W. Yan, Shield gas induced cracks during nanosecond-pulsed laser irradiation of Zr-based metallic glass, Appl. Phys. A-Mater. 122 (2016) 881.
[28] C.W. Liu, J.W. Yan, S.C. Lin, Diamond turning of high-precision roll-to-roll imprinting molds for fabricating subwavelength gratings, Opt. Eng. 55 (2016) 064105.
[29] U. Sudeep, N. Tandon, R.K. Pandey, Performance of lubricated rolling/sliding concentrated contacts with surface textures: a review, J. Tribol.-Trans. ASME 137 (2015) 031501.
[30] W.C. Oliver, G.M. Pharr, Measurement of hardness and elastic modulus by instrumented indentation: advances in understanding and refinements to methodology, J. Mater. Res. 19 (2004) 3–20.
[31] J.L. Gong, D.J. Lipomi, J.D. Deng, Z.H. Nie, X. Chen, N.X. Randall, R. Nair, G.M. Whitesides, Micro- and nanopatterning of inorganic and polymeric substrates by indentation lithography, Nano Lett. 10 (2010) 2702–2708.
[32] Y. Wang, D. Raabe, C. Kluber, F. Roters, Orientation dependence of nanoindentation pile-up patterns and of nanoindentation microtextures in copper single crystals, Acta Mater. 52 (2004) 2229–2238.
[33] H. Huang, J.L. Zhang, C.H. Shek, J.W. Yan, Effects of pre-compression deformation on nanoindentation response of $Zr_{65}Cu_{15}Al_{10}Ni_{10}$ bulk metallic glass, J. Alloys Compd. 674 (2016) 223–228.
[34] H. Huang, J.W. Yan, Investigating shear band interaction in metallic glasses by adjacent nanoindentation, Mater. Sci. Eng. A 704 (2017) 375–385.
[35] X.P. Nie, Q.P. Cao, Z.F. Wu, Y. Ma, X.D. Wang, S.Q. Ding, J.Z. Jiang, The pitting corrosion behavior of shear bands in a Zr-based bulk metallic glass, Scr. Mater. 67 (2012) 376–379.
[36] Y.M. Wang, C. Zhang, Y. Liu, K.C. Chan, L. Liu, Why does pitting preferentially occur on shear bands in bulk metallic glasses? Intermetallics 42 (2013) 107–111.
[37] W. Zhou, J.X. Hou, M.Q. Sheng, Microstructural change and corrosion behavior during rolling of Zr-based bulk metallic glass, Int. J. Electrochem. Sci. 11 (2016) 7163–7172.
[38] R. Maass, P. Birckigt, C. Borchers, K. Samwer, C.A. Volkert, Long range stress fields and cavitation along a shear band in a metallic glass: the local origin of fracture, Acta Mater. 98 (2015) 94–102.
[39] R. Maass, K. Samwer, W. Arnold, C.A. Volkert, A single shear band in a metallic glass: local core and wide soft zone, Appl. Phys. Lett. 105 (2014) 171902.
[40] A. Vinogradov, M. Seleznev, I.S. Yasnikov, Dislocation characteristics of shear bands in metallic glasses, Scr. Mater. 130 (2017) 138–142.
[41] I. Binkowski, S. Schlottbom, J. Leuthold, S. Ostendorp, S.V. Divinski, G. Wilde, Sub-micron strain analysis of local stick-slip motion of individual shear bands in a bulk metallic glass, Appl. Phys. Lett. 107 (2015).
[42] S. Kuchemann, C.Y. Liu, E.M. Dufresne, J. Shin, R. Maass, Shear banding leads to accelerated aging dynamics in a metallic glass, Phys. Rev. B 97 (2018).
[43] Y. Park, H. Jeong, S. Choi, H. Jeong, Planarization of wafer edge profile in chemical mechanical polishing, Int. J. Precis. Eng. Man. 14 (2013) 11–15.
[44] Ajay P. Malshe, Textured Surfaces to Enhance Nano-Lubrication, United States Patent, Patent No.: US 8486870B1, 2013.